JAAS

ROYAL SOCIETY OF CHEMISTRY

PAPER

View Article Online
View Journal | View Issue

Cite this: *J. Anal. At. Spectrom.*, 2025, **40**, 2945

Potassium and rubidium isotopic analysis using Neoma MC-ICPMS with the collision/reaction cell

Zhe J. Zhang, * Nicole X. Nie and Colin Z. Lin

Potassium and rubidium isotopes are critical for understanding various geological processes that shape our planet. However, their analysis often encounters significant challenges. This study introduces methods for the simultaneous purification of K and Rb using three-step ion exchange column chromatography, coupled with high-precision isotopic analyses using Thermo Fisher Scientific Neoma MC-ICPMS/MS. This instrument features a double Wien filter and a collision/reaction cell. Using an Apex Omega desolvating nebulizer and low-resolution mode, we achieved sensitivities of 345 V per ppm for ^{39}K and 800 V per ppm for ^{85}Rb and obtained high precision (≤0.05‰; 95% confidence interval) for low-concentration solutions of K (≥20 ng g^{-1}) and Rb (≥5 ng g^{-1}). Our tests indicate that K isotope measurements are largely insensitive to sample/standard concentration mismatches within ±15% but are significantly affected by acid molarity and matrix effects. In particular, elevated concentrations of Mg and Ca introduce a positive δ^{41}K bias, emphasizing the need to maintain total matrix concentrations below 2% for accurate results. Rb isotope measurements, on the other hand, show minimal sensitivity to concentration mismatch within ±20%, and various acid strength from 0.15 to 0.75 mol L^{-1} HNO_3, but are influenced by matrix effects, especially K/Rb ratios. For reliable Rb isotopic data, K/Rb ratios should be kept below 1 with 20% magnetic field of the MS/MS module (*B*-field). To validate our method, we processed geostandards through column purification, yielding isotopic compositions consistent with those from other measurement techniques. Overall, our findings demonstrate that simultaneous K and Rb isotopic analyses for low concentration samples are feasible using Neoma MC-ICPMS/MS.

Received 7th May 2025
Accepted 26th August 2025

DOI: 10.1039/d5ja00189g

rsc.li/jaas

1. Introduction

Potassium (K) and rubidium (Rb) are alkali metals constituting group I of the periodic table, each characterized by a single valence electron in their outermost shell. They share notable similarities in their chemical and physical properties: both are incompatible, moderately volatile, and fluid-mobile elements. Their incompatible nature enriches them in evolved, felsic magmas during differentiation, leading to their elevated abundances in planetary crusts relative to mantles.[1–4] Their moderate volatility is evidenced by their relatively low half-condensation temperatures (993–752 K) under nebular conditions,[5] and they can be vaporized/re-condensed during nebular and post-nebular planetary processes (*e.g.*, impact vaporization and magma degassing).[6–10] In addition, their high fluid mobility allows them to dissolve and migrate in fluid-assisted processes like weathering and hydrothermal alteration.[11–14]

Due to these unique properties, K and Rb have been investigated across a broad range of topics, providing significant insights into both high- and low-temperature processes in cosmochemistry, geochemistry, and even biology. Both elements have more than one stable or long-lived isotope, making them well-suited for isotopic studies. Advances in analytical techniques, particularly multi-collector inductively coupled plasma mass spectrometry (MC-ICPMS), have significantly improved our ability to resolve small isotopic variations of these elements in natural samples. This progress has fueled growing interest in applying K and Rb isotopes to trace planetary, geological, and biological processes.[8,15–19]

Potassium has three stable or long-lived isotopes, which are ^{39}K (93.3%), ^{40}K (0.012%), and ^{41}K (6.73%). The isotopic composition of K is commonly expressed as the ^{41}K/^{39}K ratio. Potassium-40 is a long-lived radioactive isotope that decays to ^{40}Ca and ^{40}Ar with a half-life of 1.248 billion years,[20,21] and its low abundance and the isotopic interferences from sample carrier gas (^{40}Ar$^+$) and matrix (^{40}Ca$^+$) make it challenging to measure with MC-ICPMS. However, recent studies[22,23] using thermal ionization mass spectrometry have enabled such measurements and found nucleosynthetic isotopic anomalies on ^{40}K in meteorites, but not for ^{41}K and ^{39}K. This validates using ratios of ^{39}K and ^{41}K for mass-dependent stable isotope fractionation studies.

Isotopic analysis of ^{39}K and ^{41}K with MC-ICPMS presents a great challenge due to sample carrier gas Ar, which could form ^{38}Ar^{1}H$^+$ and ^{40}Ar^{1}H$^+$ to interfere with the analysis of ^{39}K$^+$ and

CAT Lab, Department of Earth, Atmospheric, and Planetary Sciences, Massachusetts Institute of Technology, Cambridge, MA, 02139, USA. E-mail: zhez@mit.edu

$^{41}K^+$, respectively. To mitigate this interference and enhance precision, two main methods have been used, one is measuring on the interference-free peak shoulder of ^{41}K ($^{39}K^+$ is less of a problem because ^{38}Ar is a minor isotope of Ar) using hot or cold plasma.[24–31,41] K has a slightly lower mass than $^{40}ArH^+$, resulting in a very narrow, interference-free low-mass peak shoulder. Under high resolution mode, this clean region spans only 0.003–0.004 amu (atomic mass unit), representing just 1.5% of full peak width (~0.2 amu). Compared to traditional hot plasma conditions, with radio frequency (RF) power of 1200 W, cold plasma (RF power around 500–800 W) can suppress Ar-based interferences, given that Ar has a much higher ionization energy of 15.76 eV than 4.34 eV of K. However, reducing the RF power of plasma also significantly reduces the signal intensity of K. Moreover, maintaining mass stability on the narrow peak shoulder is challenging due to instrumental drift. The Neoma and upgraded Neptune Plus MC-ICPMS allow for optional "extra-high resolution" mode (XHR) that increases the mass resolving power from 9000 for HR up to 15 000 and expands the interference-free peak shoulder width to 0.006–0.007 amu.[26,29] Although XHR facilitates the analyses, it further reduces the sensitivity by a factor of 2. To compensate for this loss, desolvating nebulizer systems and jet-type sampling cones are often used to enhance sensitivity. Nonetheless, a significant amount of K is needed for high-precision isotopic measurements using this method.

The other method for high-precision K isotopic analysis involves measuring at the peak center of ^{41}K by removing nearly all ArH^+ interferences using a collision/reaction cell (CRC).[32–42] The CRC uses H_2 and He gases as the collisional gases to react with Ar-based polyatomic ions to suppress the formation of ArH^+. In principle, H_2 gas removes the proton from ArH^+ through the reaction: $ArH^+ + H_2 \rightarrow Ar + H_3^+$, and He gas acts as a mediator to promote the chance of atomic collision and accelerate the proton transfer reaction. With CRC, K isotopes can be measured at peak center under low resolution mode using hot plasma (RF power around 1200–1300 W), which gives a sensitivity of K higher by a factor of 10 compared with the peak-shoulder analyses methods mentioned above. Therefore, CRC is well-suited for analyzing small and precious samples with lower K content.

The use of CRC in analyzing the K isotopes dates back to the 2010s using a single-focus MC-ICPMS: IsoProbe from GV instruments. However, earlier studies reported unsatisfactory external reproducibility of ±0.21‰.[32,38–40] Recently, CRC technology has gained renewed attention as it is implemented in two recent commercialized MC-ICPMS: Sapphire from Nu Instruments, UK, and Neoma from Thermo Scientific, Germany. These instruments enable more precise K isotopic analysis with external reproducibility of ~±0.05‰.[33,36,37,41] The Sapphire MC-ICPMS from Nu features a dual ion path design, comprising a high energy (6 kV acceleration), conventional MC-ICPMS path and a low energy (4 kV) collision cell path. For the low energy path, ions are first extracted from the ICP, pass through the CRC (collision/reaction cell), and then re-accelerated to 4 kV and focus back to the conventional MC-ICPMS. The Neoma MC-ICPMS/MS from Thermo Scientific has only one path, with two Wien filters placed before the collision/reaction cell, which is placed before the electrostatic analyzer (ESA). Ions are first filtered according to their mass-to-charge ratios by Wien filters and then decelerated to the CRC hexapole and re-accelerated into the conventional MC-ICPMS part.

Most K isotopic studies using CRC have been conducted with the Nu Sapphire.[33,35,41,43,44] To date, only two studies have investigated K isotopic analysis on Neoma MC-ICPMS/MS. Nie *et al.*[36] carried out high-precision K isotopic analysis using a quartz cyclonic/Scott type spray chamber (wet plasma method). The wet plasma method reduces the complexity of instrument tuning and shortens washout times compared with the dry plasma method, which employs a desolvating nebulizer system to remove water. However, their results highlighted significant challenges in achieving high-precision K isotopic data with Neoma. Albalat *et al.*[37] used a dry plasma method but operated the instrument without the MS/MS module by setting both the magnetic (*B*-field) and electrical fields of the Wien filters to zero. Additionally, they used a microFAST dual-loop injection system to correct for concentration mismatch, but the system is not readily available in many labs. These limitations underscore the need for further testing of K isotopic analyses using Neoma MS/MS, particularly with dry plasma and an enabled MS/MS. In this study, we performed K isotopic measurements under these conditions to establish an optimized setup for routine high-precision K isotopic analyses using Neoma MC-ICPMS/MS.

Many studies have focused on K isotopic analysis, but research on Rb isotopes remains comparatively rare. This scarcity is not due to a lack of interest, but rather the significant challenges associated with Rb purifications using column chemistry. Indeed, combining K and Rb isotopic systems has been shown to be highly effective in tracing various processes, such as volatile loss from the Moon,[9] chondrule formation,[7] and space weathering on planetary surfaces.[10] Rb has two stable or long-lived isotopes, ^{85}Rb (72.17%) and ^{87}Rb (27.83%). Rubidium-87 decays to ^{87}Sr with a very long half-life around 48.8 billion years, and can be regarded as a stable isotope. Compared to K isotopic analyses, Rb isotopic analyses are more straightforward since Rb isotopes do not suffer from on-peak interference from carrier gas. Most Rb isotopic studies have been conducted using MC-ICPMS under low-resolution mode with either wet or dry plasma.[9,45–50] No isotopic analysis of Rb has been conducted using Neoma MC-ICPMS/MS. Given the limited understanding of how the Wien filters affect Rb isotope measurements and the lack of established tuning protocols for the MS/MS module in this context, systematic testing of Rb isotopic analysis on the Neoma MS/MS is essential. In this study, we conducted Rb isotopic tests to identify optimal methods for Rb isotopic analysis.

As stated above, the primary challenge in Rb isotopic analysis mainly arises from its purification, because: (1) the trace amounts of Rb in rocks often require larger sample digestions, which can complicate the chemistry and potentially overload the resins; and (2) its similar partition coefficients as K on most resins, making it difficult to separate both at the same time without affecting each other. Most previous studies removed K

into matrix and collected only Rb progressively at each purification step, rather than purifying both elements simultaneously.[47,49,50] Nie *et al.*[45] successfully purified both K and Rb simultaneously, but their method uses large columns that consume considerable amounts of resins and acids and is quite time-consuming. Hu *et al.*[49] used a short column but focused only Rb purification. In this study, we combined the two approaches to refine column chemistry for a more efficient, simultaneous extraction of K and Rb from the same sample. We present our test results on the purification method and isotopic analyses of K and Rb using Neoma MC-ICPMS/MS. The analyses were conducted in low-resolution mode with dry plasma to achieve the highest sensitivity, suitable for application to low-K and low-Rb samples.

2. Materials and methods

2.1 Reagents and materials

Sample preparation was carried out in the Cosmochemical Analysis and Testing (CAT) laboratory at MIT. All sample and standard preparation, as well as column chemistry, were conducted in a Class 1000 clean lab renovated in 2024. Ultrapure water was obtained from a Milli-Q® IQ 7000 system, with a conductivity of 18.2 MΩ at 25 °C and a total organic carbon content below 3.54 ppb. All acids used in this study were double distilled using the Savillex DST-1000 acid purification systems, from ACS analytical grade acids purchased from Fisher Scientific. The testing solutions used in this study were made from single-element solutions (1000 μg g^{-1} Spex CertiPrep Assurance® Grade).

To validate the accuracy of our analytical and chemical separation methods, we processed three geostandards: terrestrial basalt BCR-2, andesite AGV-2, and granite G-3. These geostandards represent a board range of igneous rock compositions. For digestion, the geostandards were treated with a 2 : 1 (v/v) mixture of double distilled HF and HNO_3 and heated at 130 °C overnight. After drying down, the residues were treated with aqua regia and heated again at 130 °C overnight. The aqua regia step was then repeated until the sample powders were fully digested.

2.2 K and Rb purification

We modified the ion-exchange chromatography protocol from Hu *et al.*[49] and Nie *et al.*[45] for K and Rb purification from silicate matrices and calibrated our approach using the geostandard AGV-2 (Fig. 1). The purification process includes three stages of column chemistry and is summarized in Table 1. The first column used PFA microcolumns (6.4 mm inner diameter) from Savillex, loaded with 2 mL pre-cleaned and conditioned AG50W-X12 cation exchange resin from Bio-Rad (200–400 mesh, hydrogen form, analytical grade). The resin in each column was initially cleaned with 20 mL of 6 M HNO_3, then conditioned with 2 mL H_2O followed by 5 mL of 1.5 M HCl for sample-loading conditioning. Sample solutions in 1 mL of 1.5 M HCl were loaded onto the resin columns, and eluted first with a mixture of 5 mL of 1.5 M HCl and 0.5 M HF, followed by 8 mL of 1.5 M HCl to remove major elements such as Ti, Al, and Fe along with other matrix elements. K and Rb were collected in a subsequent 22 mL elution of 1.5 M HCl, together with some Mn. At some cases, trace Mg

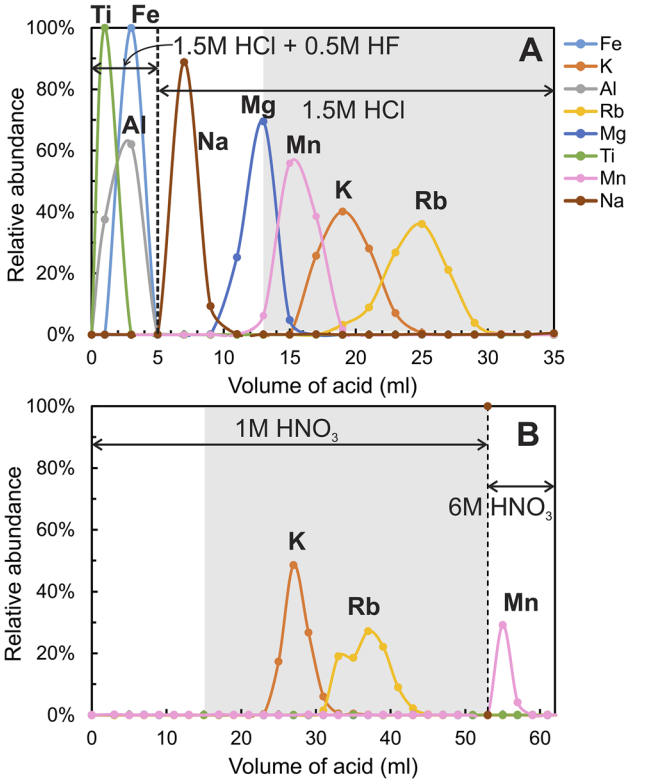

Fig. 1 Elution curves of major elements for geostandard andesite AGV-2 for column 1 (panel A). The purification procedure for column 1 is modified from Hu *et al.*[49] The obtained elution curves are consistent with those reported for different rock standards in Hu *et al.*[49] The collected K–Rb elution cut from column 1 was then passed through column 2, with elution curves shown in panel B. Most rock-forming elements (*i.e.*, Ti, Fe, Al, Na, Mg) were sufficiently removed after column 1 except Mn, which is later removed in column 2. The relative abundance is the percentage of collected amount for an element relative to the amount loaded on column 1.

remain in the K and Rb elution. A repeat of the first column may be performed, if necessary, to further remove Mg. After these steps, this eluate containing K, Rb and some Mn was dried, treated with concentrated HNO_3 to eliminate residual chloride, and then redissolved in 1 mL of 1 M HNO_3, ultrasonicated, and heated at 130 °C until fully dissolved.

The second stage purification reused columns from the first stage. These columns were cleaned with 20 mL of 6 M HNO_3, reconditioned with 5 mL H_2O and 5 mL of 1 M HNO_3, and reloaded with the purified K and Rb solutions from the first step. Matrix elements were first eluted with 15 mL of 1 M HNO_3, while K and Rb were subsequently collected using 35 mL of 1 M HNO_3. At this stage, Mn remained bound to the resin and was removed from the K-Rb cut.

The third column used a PFA microcolumn (4.5 mm inner diameter, 40 cm length) from Savillex filled with Srspec resin from Eichrom. The resin was cleaned with H_2O and conditioned with 5 mL of 3 M HNO_3. Samples in 0.5 mL of 3 M HNO_3 were loaded onto the columns, and the matrix was eluted with 3.9 mL of 3 M HNO_3. Rb was then collected in the next 12 mL of 3 M HNO_3, and K in the subsequent 20 mL of 3 M HNO_3. Details on the elution profiles for column 3 are provided in Nie *et al.*[45]

Table 1 Elution procedure of K and Rb purification for rock samples

Column 1, AG50W-X12 resin, 200–400 mesh, 2 mL in Savillex PFA microcolumn (6.4 mm ID)			
Conditioning	5 mL	1.5 M HCl	
Sample loading	1 mL	1.5 M HCl	
Elution of matrix	5 mL	1.5 M HCl + 0.5 M HF	
Elution of matrix	8 mL	1.5 M HCl	
Elution of K and Rb	22 mL	1.5 M HCl	Contains Mn
Column 2, AG50W-X12 resin, 200–400 mesh, 2 mL in Savillex PFA microcolumn (6.4 mm ID)			
Conditioning	5 mL	1 M HNO_3	
Sample loading	1 mL	1 M HNO_3	
Elution of matrix	15 mL	1 M HNO_3	Mn remains on column
Elution of K and Rb	35 mL	1 M HNO_3	Mn remains on column
Column 3, Sr resin, 50–100 μm size, in Savillex PFA microcolumn with 40 cm length (4.5 mm ID)			
Conditioning	5 mL	3 M HNO_3	Elution at 2.5 psi pressure with linear flow rate of ~0.38 cm min^{-1}
Sample loading	0.5 mL	3 M HNO_3	
Elution of matrix	3.5 mL	3 M HNO_3	
Elution of Rb	12 mL	3 M HNO_3	
Elution of K	20 mL	3 M HNO_3	

The recovery and blanks of the entire purification procedure were carefully examined. The total yield for both K and Rb is higher than 95%, and the total procedure blank was <0.38 μg for K and <0.05 ng for Rb, which are negligible relative to the total K and Rb in samples (less than 0.1%).

2.3 K and Rb isotopic measurements

Both K and Rb isotopic ratios were measured using a Neoma MC-ICPMS/MS installed in January 2025 in the CAT lab at MIT. The K solutions in 0.3 mol L^{-1} HNO_3 were introduced into the MC-ICPMS using an APEX Omega desolvating nebulizer with a flow rate of 150 μL min^{-1}. Normal Ni sampler and skimmer cones were used, and all analyses were carried out under low resolution (around 2200 mass resolving power for 5–95% on ascending edge). The cup configuration for K is listed in Table 2, with each Faraday cup equipped with a 10^{11} Ω amplifier. Before each measurement, the signal was tuned following the procedures outlined in Nie *et al.*,[36] to obtain good sensitivity and stability of K signals. Helium and H_2 gases were used in CRC to remove ArH^+ interferences. The detailed tunning parameters for K are given in Table 3.

The Rb isotopic measurements were also carried out on the Neoma MC-ICPMS/MS using low resolution mode, but without any gases in the collision/reaction cell. Normal Ni sampler and X skimmer cones were used to achieve better sensitivity due to the lower abundance of Rb compared to K. The Rb solutions in 0.3 mol L^{-1} HNO_3 were introduced into the Neoma MC-ICPMS/MS using the APEX Omega desolvating nebulizer with a flow rate around 150 μL min^{-1}. The cup configuration for Rb is listed in Table 2 with each cup equipped with a 10^{11} Ω amplifier. The details of tunning parameters for Rb are given in Table 3.

Throughout this study, concentrations are expressed in ppm (equivalent to μg g^{-1}) and ppb (equivalent to ng g^{-1}) units for consistency. Sample solutions of both K and Rb were analyzed using the sample-standard bracketing technique to correct for instrumental fractionation. Acid blanks were measured before and after every 4 samples to monitor and correct for the blank. Each measurement consisted of 40 repeats, with a 4 second integration time per repeat. The wash time was set to 90 seconds, and the take-up time was 110 seconds. Each sample or standard solution was analyzed 5–9 times as replicates, and the averaged value was taken. The uncertainty for each sample was calculated using either 2SD or 95% confidence interval assuming a student t distribution. $^{40}Ca^+$ was monitored during K analysis to evaluate Ca interference. For Rb isotopes, the contribution of $^{87}Sr^+$ on $^{87}Rb^+$ was corrected for using the measured $^{88}Sr^+$ and a constant $^{87}Sr/^{88}Sr$ ratio of 0.085 when minor amounts of Sr were presented ($^{88}Sr/^{85}Rb$ must be lower than 0.001 for accurate $\delta^{87}Rb$ measurements).[9] Results for K and Rb measurements are reported in delta notations, which are per mil deviations from the standards SRM 999c for K, which has the same $\delta^{41}K$ as the reference material SRM 3141a,[24] and SRM 984 for Rb:

Table 2 Cup configurations for K and Rb isotopic analyses

	Cups										
Elements	L5	L4	L3	L2	L1	C	H1	H2	H3	H4	H5
K	^{38}Ar		^{39}K		^{40}Ar ^{40}Ca	^{41}K	^{42}Ca		^{43}Ca		^{44}Ca
Rb		^{83}Kr	^{84}Sr	^{85}Rb	^{86}Sr	^{87}Rb	^{88}Sr	^{90}Zr	^{92}Mo	^{94}Mo	

Table 3 The tunning parameters for Neoma MC-ICPMS/MS using Apex Omega for K and Rb isotopic analyses

	K	Rb
Apex Omega		
Ar flow rate (L min^{-1})	6.01	5.40
N_2 flow rate (mL min^{-1})	0	2.25
Spray chamber (°C)	140	140
Peltier (°C)	3.0	3.0
Desolvator (°C)	155	155
Peripump (μL min^{-1})	783	600
Neoma-ICP		
Plasma power (W)	1200	1200
Source slit	Low resolution	Low resolution
Torch horizontal position (mm)	−0.36	−0.49
Torch vertical position (mm)	−0.87	−0.74
Torch sampling depth (mm)	6.0	4.0
Cool gas flow (L min^{-1})	14	14
Auxiliary gas flow (L min^{-1})	0.9	0.9
Nebulizer gas flow (L min^{-1})	1.145	1.035
Neoma-lenses		
Focus (%)	44.5	47.5
X deflection (%)	−4.85	−5.8
Y deflection (%)	−0.2	−0.8
Shape (%)	59.6	61.0
Neoma -CRC		
Helium (mL min^{-1})	1.5	0
Hydrogen (mL min^{-1})	5.0	0
CCT lenses entry (V)	−44	−47
CCT lenses bias (V)	−9.0	−2.4
CCT lenses RF amplitude (%)	100	100
CCT lenses exit 1 (V)	−19	−85
CCT lenses exit 2 (V)	−82.0	−100
Neoma-MSMS		
Magnetic field (%)	10	20
Electric field (V)	73.4	103.8
Slit opening (%)	100	100
Pre-filter focus lens 1 base (V)	−476.0	−450
Pre-filter focus lens 1 X-symmetry (V)	4.0	8.0
Pre-filter focus lens 1 Y-symmetry (V)	−1.0	−4.0
Pre-filter focus lens 2 base (V)	−446	−425
Pre-filter focus lens 3 base (V)	−367	−380
Pre-filter focus lens 3 X-symmetry (V)	−8.0	−13.0
Pre-filter focus lens 3 Y-symmetry (V)	−3.0	−3.0

$$\delta^{41}\mathrm{K}\ (‰) = [(^{41}\mathrm{K}/^{39}\mathrm{K})_{\mathrm{sample}}/(^{41}\mathrm{K}/^{39}\mathrm{K})_{\mathrm{SRM999c}} - 1] \times 1000. \quad (1)$$

$$\delta^{87}\mathrm{Rb}\ (‰) = [(^{87}\mathrm{Rb}/^{85}\mathrm{Rb})_{\mathrm{sample}}/(^{87}\mathrm{Rb}/^{85}\mathrm{Rb})_{\mathrm{SRM984}} - 1] \times 1000. \quad (2)$$

3. Results and discussion

3.1 Sensitivity of K and Rb, and the effect of concentration on analytical precision

High-precision isotopic ratio analyses require high signal-to-noise ratios, which can be improved by increasing ion beam intensity during measurements. Ion beam intensity is governed by the amount of sample introduced into the ICP source and the ionization-transmission efficiency (TIE). For MC-ICPMS, ionization efficiency approaches 100% due to the high temperature of the Ar plasma. Therefore, transmission efficiency is typically the limiting factor for ion beam intensity, and is influenced by many parameters such as nebulizer types, the geometry of the sampler/skimmer cones, vacuum conditions, beam alignment, and lens settings. While many previous studies report sensitivity as volts per part per million (V per ppm), this metric reflects only signal intensity and does not account for TIE. In the following discussion, we report the sensitivity in both TIE and V per ppm to enable direct comparison with prior work.

The beam intensity for ^{39}K in this study was approximately 345 V for 1 μg g^{-1} K standard solution (V per ppm) with standard Ni sampler and skimmer cones, and APEX Omega desolvating nebulizer. It converts to 0.060% of TIE with 150 μL min^{-1} uptake rate in this study. There is a trade-off between sensitivity and stability. We prioritized stability over maximum signal intensity. The obtained sensitivity is comparable to 0.052–0.078% TIE (200–300 V per ppm) reported by Nie *et al.*[36] using Jet sampler and X skimmer cones and wet plasma. In contrast, Albalat *et al.*[37] achieved a sensitivity of 0.261% TIE (~1000 V per ppm) using Jet sampler and X skimmer cones and dry plasma. Given our use of standard Ni sampler and skimmer cones, we estimate that replacing them with Jet and X cones could increase sensitivity by a factor of 2–3, bringing it closer to the values reported by Albalat *et al.*[37] Overall, the sensitivity range of ^{39}K for Neoma MC-ICPMS/MS (200–1000 V per ppm) seems to be lower than that reported for Sapphire CRC-MC-ICPMS (750–2000 V per ppm).[33,35,41] Although decreasing the flow rate of H_2 and He in the collision cell can increase the ^{39}K sensitivity to as much as 1000 V per ppm in our tests, it also increased the ArH^+ interferences and negatively impacted the isotopic analyses. Therefore, we maintained our tuning settings at the 345 V per ppm sensitivity level for K isotopic analyses.

Despite the relatively moderate sensitivity, we achieved sufficient precision for K concentration as low as 20 ppb (Fig. 2). The effect of K concentration on analytical precision was tested using 20 ppb, 50 ppb, 100 ppb, and 200 ppb standard solutions in 0.3 mol L^{-1} HNO_3 (Fig. 2). The obtained precision was compared with the theoretical limits from Johnson noise and counting statistics, calculated using the original formula from Dauphas *et al.*[51] and the modified equations from Dauphas *et al.*[52] that account for acid blank correction. The obtained uncertainties in this study remained constant with increasing concentration and were all plotted above the theoretical limits from Johnson noise and counting statistics. This indicates that additional sources of uncertainties exist, potentially arising from sample introduction (plasma, the double Wien filter, and/or the collision/reaction cell). This was also observed in Nie *et al.*[36]

Nie *et al.*[36] carried out K isotopic analyses on Neoma MC-ICPMS/MS using a wet plasma method, and they observed a significant precision loss when K concentration changed while maintaining the same tuning parameters within one session of measurement. For example, when the instrument was optimally tuned for 250 ppb K solutions, reducing the

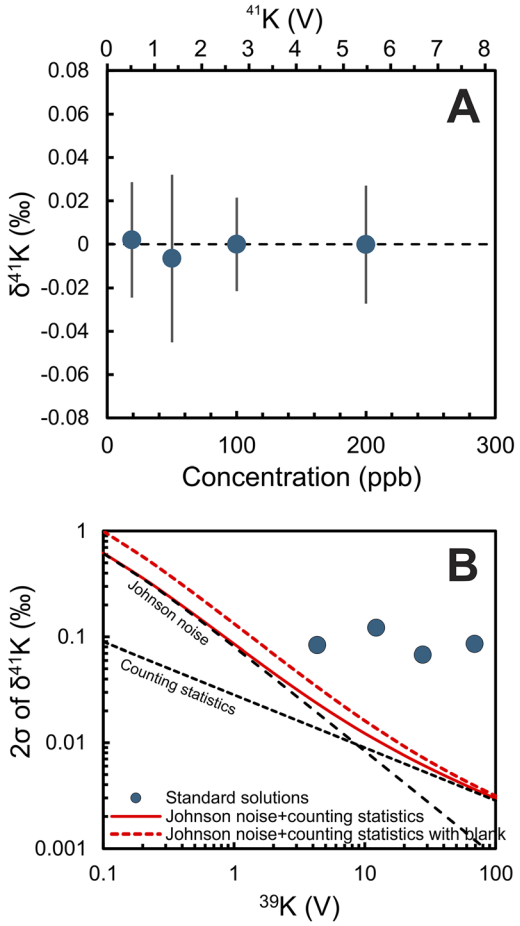

Fig. 2 Accuracy and precision of K isotopic analysis for different K concentrations of 20 ppb, 50 ppb, 100 ppb, and 200 ppb (panel A). The obtained uncertainties are compared with theoretical limits from Johnson noise and counting statistics based on equations from Dauphas *et al.*[51] (Panel B). The dashed black lines in panel B are Johnson noise and counting statistics, respectively. The red solid line is a combination of these two sources of errors. The red dashed line takes into account the blank measurements following methods from Dauphas *et al.*[52] The signal intensity of blanks is variable and depends on many factors, *e.g.*, the duration of analysis, the concentration of the standard/sample solutions, and the cleanness of the Apex Omega desolvating nebulizer and cones. In this study, an averaged value of 0.79 V for ^{39}K was used for background signals.

concentration to 200 ppb led to a substantial decline in both accuracy and precision, increasing the uncertainty from 0.050‰ to 0.924‰. Such phenomenon was not observed in this study, which we attribute to differences in our use of dry plasma *vs.* their use of wet plasma. Albalat *et al.*[37] observed interferences on the high-mass shoulder of the ^{39}K and ^{41}K peaks, which are likely due to the formation of complex organic compounds in the collision cell. We similarly observed interferences on the higher-mass shoulder of ^{39}K, especially when using N_2 in the Apex Omega desolvator system. To mitigate this effect, we applied a −0.0068 amu offset (~9.7% of total peak width: 0.070 amu) to the center cup (^{41}K) relative to the peak center when measuring K isotopes.

The sensitivity of ^{85}Rb was about 800 V per ppm using the normal Ni sampler and X skimmer cones with dry plasma on the Neoma MC-ICPMS/MS, which translates to 0.446% TIE. This is lower than the 0.986% TIE (650 V per ppm) reported by Zhang *et al.*[46] for the Neptune Plus MC-ICPMS using similar cones combination and dry plasma with 50 μL min^{-1} uptake rate, but comparable to the ~0.372% TIE (~500 V per ppm) achieved with Nu Sapphire MC-ICPMS (standard Ni cones, dry plasma, and 100 μL min^{-1} uptake rate).[18] Zhang *et al.*[46] carried out tests on different cone combinations and their associated effects on analytical precisions. They found that although Jet + X cones yielded the highest sensitivity (~750 V per ppm), it also significantly increased the measurement uncertainties from ±0.05 to ±0.11‰, compared with Normal Ni + X cones. They suggested the optimal combination to be Ni sampler + X skimmer cones, which was adopted in this study.

The effect of Rb concentration on analytical precision was tested in this study using Rb standard solutions in 0.3 mol L^{-1} HNO_3, with concentration ranging from 2 ppb to 50 ppb, corresponding to 0.5–20 V for ^{87}Rb. The results showed good precision and accuracy, with uncertainties below 0.033‰ (95%

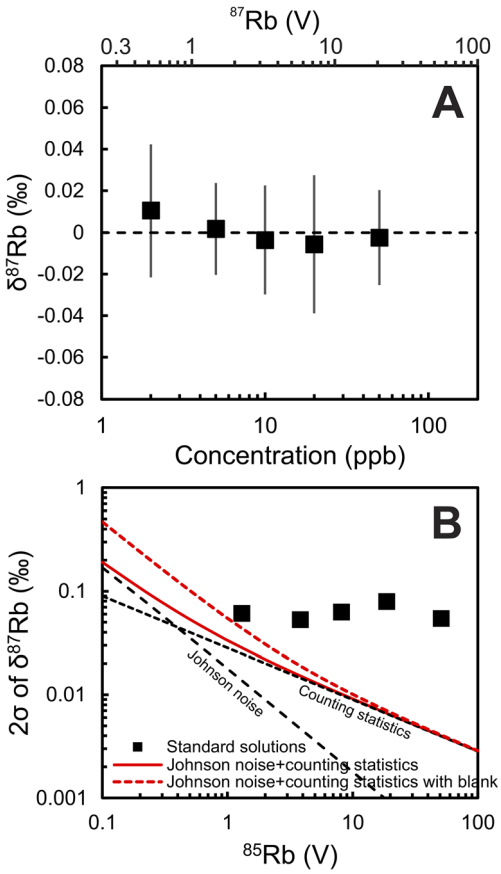

Fig. 3 Rb isotopic analysis for different Rb concentrations of 2 ppb, 5 ppb, 10 ppb, 20 ppb and 50 ppb (panel A). The uncertainties are compared with theoretical limits from Johnson noise and counting statistics based on equations from Dauphas *et al.*[51] (panel B). Details of theoretical limits are given in the caption of Fig. 2. An averaged value of 0.11 V for ^{85}Rb was taken as the blank value for the calculation of dashed red line.

confidence interval) even at the lowest tested Rb concentration of 2 ppb (Fig. 3). When compared with the theoretical limits calculation from Johnson noise and counting statistics, the obtained precisions exceed the theoretical limit (Fig. 3B) and do not correlate with signal intensities, which are similar to K isotopic analysis, suggesting additional error sources.

In summary, our study achieved remarkable precision in Rb isotopic analysis, reaching an uncertainty of ±0.03‰ at a 95% confidence interval for concentrations as low as 2 ppb. Under these conditions, only ~10 ng of Rb or less is required for 9 replicate measurements. For context, an average Mid-Ocean Ridge Basalt (MORB) sample contains 2.88 ppm of Rb and 0.16 wt% K_2O,[53] which means that only 4.2 mg of material is needed for Rb isotopic analysis. This sample amount yields approximately 1344 μg of K, substantially more than the 0.3 μg needed for K isotopic analysis. The high precision and minimal mass requirements significantly reduce the amount of sample needed, enabling the analysis of both terrestrial and extraterrestrial samples that are precious or highly volatile depleted.

3.2 Effect of concentration mismatch

The effect of concentration mismatch on K and Rb isotopic analyses was examined using bracketing standards of 41 ppb K and 10 ppb Rb in 0.3 mol L^{-1} HNO_3, respectively. The K concentrations of samples deviated from the bracketing standards by a large range of ~±15%. The results showed that K isotopic measurements were not sensitive to concentration mismatch when the pre-filter magnetic field (*B*-field) was set to 10% (Fig. 4A). This finding is consistent with Nie *et al.*,[36] who used a *B*-field of 30%, and comparable to Albalat *et al.*,[37] who conducted measurements with the MS/MS module disabled (*B*-field = 0%) (Fig. 4). Albalat *et al.*[37] observed a positive linear correlation between the extent of K concentration mismatch and δ^{41}K values, resulting in up to 0.5‰ offset for δ^{41}K with 20% mismatch between samples and standards. They further noted that the slope of this correlation depends on instrument tuning parameters, indicating that the effect arises from the settings of the instruments. Similar effects have also been observed in analyses using the Nu Sapphire CRC-MC-ICPMS.[27,33–35,41,54] In this study, mismatches were limited to <15%, lower than the ±20% from Albalat *et al.*[37] Within this range, we did not observe significant effects or correlations between δ^{41}K and concentration offsets, similar to Nie *et al.*[36] and Albalat *et al.*[37] However, the influence of concentration mismatch may become more pronounced at values >15%. Based on this study and previous work,[36,37] the MS/MS module (*i.e.*, the *B*-field/*E*-field) does not appear to significantly affect the concentration mismatch effect on K isotopic analysis.

Concentration mismatch tests for Rb isotopes were conducted under two conditions: 20% and 0% *B*-field to evaluate the effect of the MS/MS module. Under MS/MS-disabled conditions (*B*-field = 0%), the sensitivity of ^{85}Rb decreased from 800 V per ppm to 650 V per ppm, although measurement precision remained unchanged compared with normal setting (*B*-field = 20%). As shown in Fig. 4B, there is no significant difference between the two settings, indicating that Rb isotope

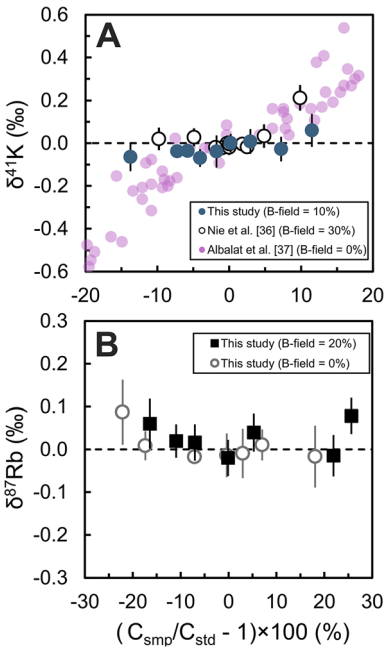

Fig. 4 Effects of concentration mismatch on K and Rb isotopic measurements. K isotopic measurements were carried out with *B*-field = 10% and compared with literature data using the same instrument but under different *B*-field conditions (30% for Nie *et al.*;[36] 0% for Albalat *et al.*[37]). Rb isotopic measurements were carried out under two different conditions: with MS/MS module enabled (*B*-field = 20%) and disabled (*B*-field/*E*-field = 0). The bracketing standards are 41 ppb K solution and 10 ppb Rb solution for K and Rb isotopes, respectively. The results show that K isotopic compositions are unaffected by up to ±15% concentration mismatch between samples and standards, and Rb isotopic results remain stable up to ±20% mismatch.

ratios are insensitive to concentration mismatch regardless of whether the MS/MS module is enabled. This contrasts with K isotopes, which showed some dependence on the instrument tuning parameters.[37] The observed insensitivity for Rb is consistent with previous studies, which have reported that Rb isotope ratios are unaffected by concentration mismatches of up to ±20% using wet plasma and up to ±50% using dry plasma.[18,46,49]

3.3 Effect of K and Rb acid molarity mismatch

The effect of acid molarity mismatch on K and Rb isotopic ratios was examined using 50 ppb K and 10 ppb Rb sample solutions in different molarities of HNO_3 (0.15, 0.30, 0.45, 0.60, and 0.75 mol L^{-1}). The bracketing standards were prepared at the same concentrations as the samples but in 0.45 mol L^{-1} HNO_3 solutions. The results showed a negative correlation between δ^{41}K and the acid molarity. Solutions with higher acid molarities have δ^{41}K shifted to more negative values and *vice versa* (Fig. 5C). Compared to a previous study using wet plasma,[36] which observed a significant deviation of δ^{41}K up to −5‰ using 0.15 mol L^{-1} HNO_3, the effect in our study is much smaller, with δ^{41}K shifted by ~0.2‰ in 0.15 or 0.75 mol L^{-1} HNO_3. Albalat *et al.*[37] found no effects on K isotopic measurement with different acid molarities. The effect of HNO_3 concentration on

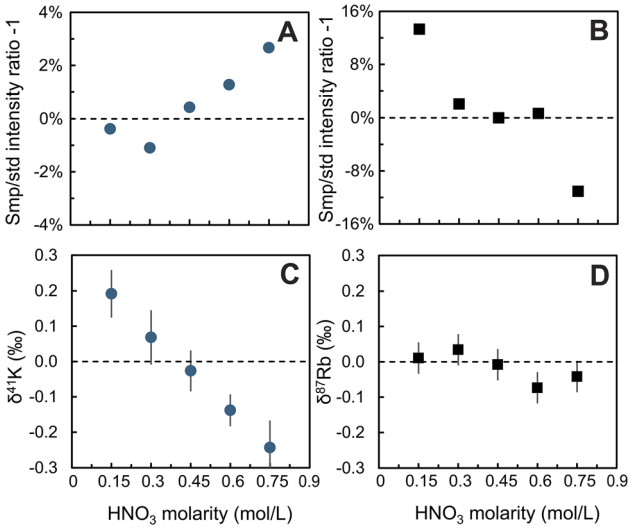

Fig. 5 Effects of acid molarity mismatch on the signal intensities and isotopic compositions of K (panels A & C) and Rb (panels B & D, respectively). The samples and standards are 50 ppb K and 10 ppb Rb solutions. Samples were prepared with varying acid molarities from 0.15 to 0.75 mol L^{-1}, but the bracketing standards were in 0.45 mol L^{-1} HNO_3.

δ^{41}K is quite variable in literature. Some studies reported no effects,[26,29,37,41] while others reported significant effects,[28,33–35] regardless of whether collision cells are used. Based on our tests, dry plasma seems to mitigate this effect compared to wet plasma.[36]

For Rb isotopes, acid molarity has a larger effect on signal intensity (up to 14% difference), but less impact on δ^{87}Rb values (Fig. 5). The insensitivity of Rb isotopes to acid molarity were also reported by other studies.[18,46]

3.4 Matrix effects

Matrix effects on K isotopic analysis were examined by doping the same K solution with major rock-forming elements Na, Mg, Fe, and Ca. Sample solutions and bracketing standards were prepared with 50 ppb K in 0.3 mol L^{-1} HNO_3 and doped at concentrations of 0.5, 1, 2.5 and 5 ppb for Na, Mg, Fe and Ca. Our results indicate minimal changes in δ^{41}K values (less than 0.1‰) with the addition of Na and Fe up to 10% (Fig. 6). Previous studies have suggested that potential interferences from $^{23}Na^{16}O^+$ on ^{39}K and $^{23}Na^{18}O^+$ on ^{41}K could cause a negative deviation of δ^{41}K (Fig. 6A).[27,36] However, our findings do not reproduce this effect. In contrast, Albalat *et al.*[37] reported a positive offset in δ^{41}K for their Na-doping experiments using the Neoma MC-ICPMS/MS, though the cause remains unclear.

A large matrix effect was observed with Ca, where δ^{41}K showed a progressive positive deviation up to +0.4‰ for 10% Ca addition (Fig. 6D). This is likely due to the formation of $^{40}CaH^+$ in the presence of H_2 collision gas, causing isotopic interference on ^{41}K. This effect is consistent with other studies utilizing collision/reaction cells but was not seen in studies using peak-shoulder measurements with XHR mode,[26,27,29] confirming that H_2 gas used in collision cells is the main cause. Mg caused a notable positive deviation in δ^{41}K up to 0.4‰ for a 10% addition (Fig. 6B). These deviations were also observed by Nie *et al.*[36] using a wet plasma setting and by Albalat *et al.*[37] using a dry plasma, both employing the Neoma MC-ICPMS/MS. Nie *et al.*[36] attributed this effect to the formation of $^{25}Mg^{16}O^+$ interference on ^{41}K and a lesser interference of $^{25}Mg^{14}N^+$ on ^{39}K.

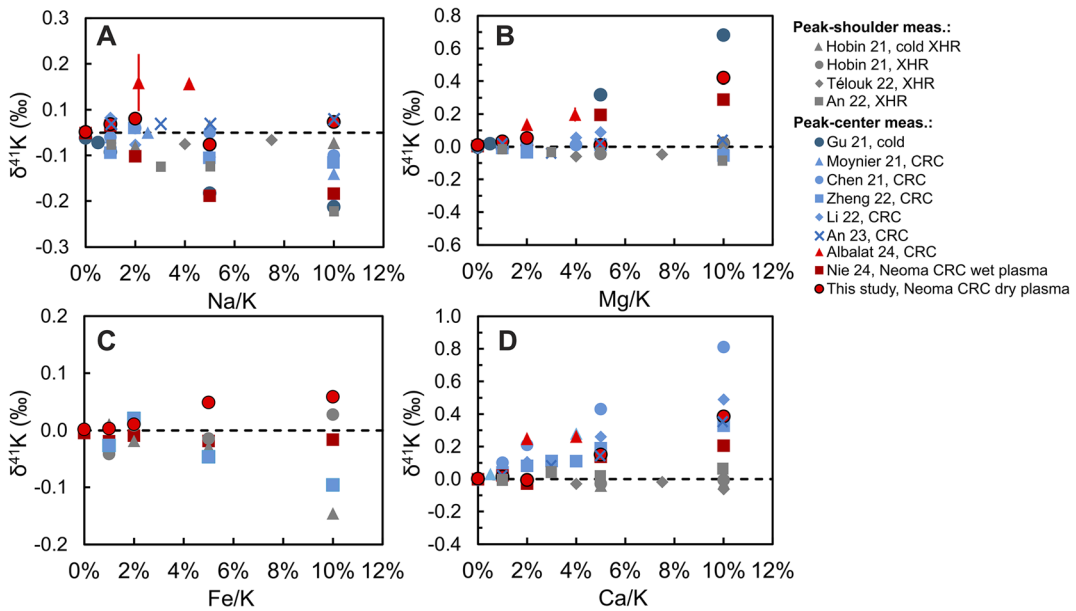

Fig. 6 Matrix effects on K isotopic measurements in presence of Na (A), Mg (B), Fe (C) and Ca (D), compared with literature data. Sample and bracketing standard solutions were 50 ppb K solutions. Sample solutions were doped with variable amount of a matrix element ranging from 0.5 ppb to 5 ppb. The results are compared with previous measurements conducted under two different setting: (1) measurements on peak shoulder of ^{41}K using ultra-high-resolution mode (XHR), and (2) measurements on peak center of ^{41}K using either a collision reaction cell or cold plasma. Our results are plotted as red-filled circles.

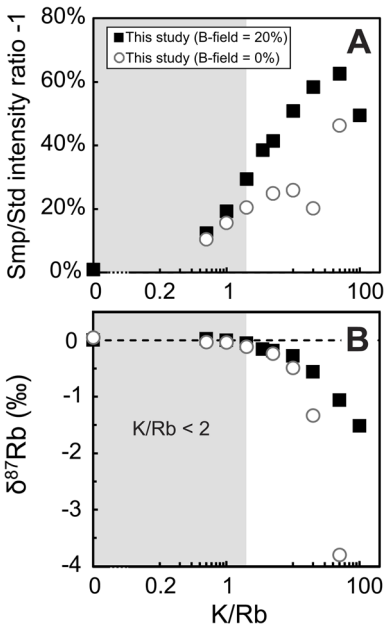

Fig. 7 Influence of K matrix on Rb isotopic analyses. Measurements were conducted under two conditions: with MS/MS module enabled (*B*-field = 20%) and disabled (*B*-field and *E*-field = 0), while all other parameters are optimized for signal intensity. A 10 ppb Rb standard solution was doped with varying amounts of K to produce K/Rb ratios ranging from 0 to 100. In both cases, increasing the K/Rb ratio enhanced the Rb signal intensity and lowered the δ^{87}Rb. However, when the MS/MS module was disabled, δ^{87}Rb values became more negatively biased with increasing K, indicating a stronger matrix effect. Enabling the double Wien filter mitigates the influence of low-mass interferences (*i.e.,* K) on Rb isotope measurements. Accurate results were achieved when the MS/MS module was enabled and the K/Rb ratio was maintained below 2.

However, such interference was not reported in studies using the Nu Sapphire CRC-MC-ICPMS[35,41] or the Neptune MC-ICPMS,[25,31] which lack mass filters (Fig. 6). This suggests that the observed matrix effect of Mg may be specific to the MS/MS module of Neoma. It is possible that the MS/MS module has promoted the effect of $^{25}Mg^{16}O^{+}$ and $^{25}Mg^{14}N^{+}$, but further investigations are needed to understand these discrepancies.

For Rb isotopes, the major concern is matrix element K (except for Sr, which has ^{87}Sr that interferes directly with ^{87}Rb and must be removed quantitatively). Other major rock-forming elements (*e.g.*, Na, Fe, Mg) can be efficiently removed by chemical purification but K follows Rb closely on columns and separating the two completely from each other is challenging. Due to large K/Rb ratios in rocks (~200),[4] insufficient separation between K and Rb has a much larger impact on Rb than on K. To test matrix effect of K on Rb isotopic analyses, we prepared the sample solutions using 10 ppb Rb in 0.3 mol L^{-1} HNO_3 and doped with variable amount of K, with K/Rb ratios varying from 0.5 to 100. The experiments were conducted under two MS/MS conditions with 20% and 0% *B*-field settings to compare the effect of Wien filters. The results are shown in Fig. 7. Under the 20% *B*-field condition, the addition of K increased the Rb signal intensity by up to 60% and shifted the δ^{87}Rb value to as low as −1.6‰. Under the 0% *B*-field condition, the presence of K had a more pronounced effect, driving δ^{87}Rb values down to −4‰ at a K/Rb ratio of ~50. These results indicate that the enabled MS/MS module effectively filters out lower-mass species such as K^{+}, thereby reducing matrix effects on Rb isotope measurements. To ensure accurate Rb isotopic analysis, we recommend operating the MS/MS module with a 20% *B*-field and maintaining the K/Rb ratio in the sample below 2. This upper limit is much lower than the K/Rb ratio of <50 suggested by Nie and Dauphas.[9] However, Nie and Dauphas[9] used wet plasma on Neptune MC-ICPMS, which may have higher tolerance compared to the dry plasma on Neoma MC-ICPMS/MS used in this study. Other studies suggested various limits: K/Rb < 20 using the high energy path (no collision cell) of Nu Sapphire MC-ICPMS,[18] K/Rb < 2 using wet plasma on Neptune Plus MC-ICPMS,[50] K/Rb < 8 suggested by Zhang *et al.*[46] using dry plasma and Neptune Plus MC-ICPMS, and K/Rb < 1.5 using wet plasma and Neptune Plus MC-ICPMS.[49] From a practical standpoint, ensuring a K/Rb ratio <1 would be ideal for Rb isotopic analysis.

3.5 K and Rb isotopic compositions of geological standards

For K isotopic analyses, we measured two batches of samples. The first batch consisted of K solutions of geostandards, which had been previously purified using a four-step ion exchange column chromatography[8] and was analyzed using cold plasma

Table 4 The K and Rb isotopic compositions of geostandards and comparison with literature data

Sample	δ^{41}K (‰)	2SD	95% c.i.	*N*	δ^{41}K (‰) literature	δ^{41}K (‰) uncertainties
AGV-2[a]	−0.445	0.124	0.052	8	−0.45[d]	0.11[d]
G-3[a]	−0.523	0.173	0.091	6	−0.439[c]	0.033[c]
BCR-2[a]	−0.469	0.100	0.053	6	−0.49[d]	0.18[d]
BHVO-2[b]	−0.378	0.083	0.039	7	−0.46[d]	0.09[d]
W-2[b]	−0.431	0.092	0.039	8	−0.48[d]	0.20[d]
G-A[b]	−0.477	0.077	0.036	7	−0.435[c]	0.042[c]
BE-N[b]	−0.348	0.097	0.045	7	−0.396[c]	0.046[c]
GS-N[b]	−0.446	0.104	0.065	5	−0.46[d]	0.04[d]
GSR-1[b]	−0.440	0.139	0.047	11	−0.527[c]	0.045[c]

[a] Sample digested and proceeded in CAT lab at MIT following the method described in Section 2.2. [b] Sample solutions from Nie *et al.*[8] [c] Data are from Nie *et al.*[8] and uncertainties are reported as 95% confidence interval. [d] Data are from Wang *et al.*[15] and uncertainties are reported as 2SD.

Table 5 Rubidium isotopic compositions of geostandards

Sample	δ^{87}Rb (‰)	2SD	95% c.i.	N	δ^{87}Rb^b (‰) literature	δ^{87}Rb^b (‰) 95% c.i.
AGV-2^a	−0.12	0.078	0.039	10	−0.13	0.02
G-3^a	−0.21	0.114	0.057	9	−0.23	0.03
BCR-2^a	−0.16	0.096	0.048	9	−0.16	0.02
GS-N^a	−0.16	0.088	0.046	9	−0.14	0.05

^{a} Sample digested and proceeded in CAT lab at MIT following the method described in Section 2.2. ^{b} Literature values and their uncertainties are from Nie *et al.*[45]

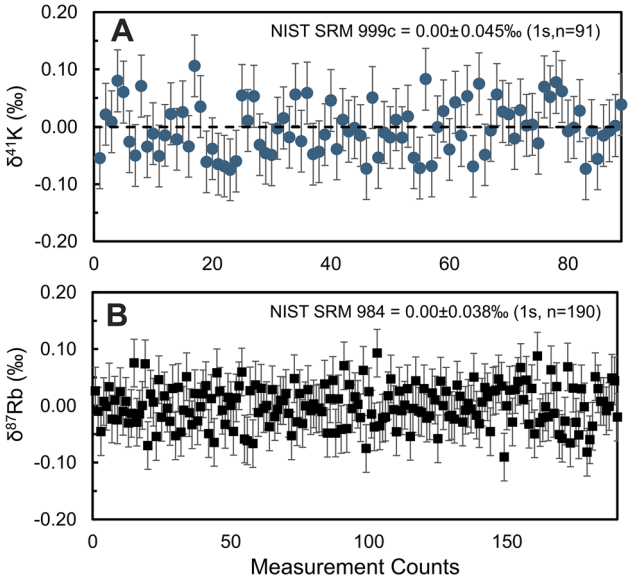

Fig. 8 The long-term stability (6 months) of the δ^{41}K and δ^{87}Rb values for bracketing standards SRM 999c and SRM 984, respectively.

setting on Nu Plasma MC-ICPMS at the University of Washington. The second batch comprised three geostandards that were digested and purified at the CAT lab using the chemistry described in Section 2.2, yielding both K and Rb. These geostandards were measured at 50 ppb K, notably lower than the concentrations used in previous studies (300 ppb in Nie *et al.*;[36] 200 ppb in Albalat *et al.*;[37] and 1000 ppb using XHR methods in Télouk *et al.*[26]). We maintained concentration match within 2%, and the intensity ratio of ^{40}Ca to ^{39}K was kept under 0.02, indicating a Ca matrix contribution of <2%. For Rb isotopic analysis, a concentration of 20 ppb was used. The results for K and Rb isotopes are given in Tables 4 and 5, respectively, and compared with literature values.[8,15,45] The isotopic values obtained in this study align with established literature values, demonstrating the accuracy of our analytical procedure.

The long-term stability and repeatability for K and Rb isotopic analyses were evaluated by compiling the δ^{41}K and δ^{87}Rb values of the bracketing standards SRM 999c (K, 50 ppb) and SRM 984 (Rb, 20 ppb), respectively, for different analytical sessions over 6 months. The results are plotted in Fig. 8. The obtained δ^{41}K values for SRM 999c and δ^{87}Rb values for SRM 984 are 0.00 ± 0.09‰ (2SD, n = 91) and 0.00 ± 0.076‰(2SD, n = 190) respectively.

4. Conclusions

In this study, we performed tests on isotopic analyses of K and Rb using the newly installed Neoma MC-ICPMS/MS in the CAT lab at MIT. The Neoma MC-ICPMS/MS is equipped with a double Wien filter and a collision/reaction cell (*i.e.*, the MS/MS option). Our results indicate that K isotopic analysis can be conducted with dry plasma to achieve high accuracy and precision of ~0.05‰ (95% confidence interval) at concentrations as low as 20 ppb, with a sensitivity of 0.060% TIE (345 V per ppm). This is primarily due to the effective removal of ArH^+ by H_2 gas in the collision/reaction cell. The isotopic analysis of K is unaffected by concentration mismatches of up to ±15%, shows minor effects from variations in acid molarity, and is more influenced by the presence of matrix elements Mg and Ca. Our Rb isotopic analysis had a sensitivity of 0.446% TIE (800 V per ppm) with normal Ni sampler and X skimmer cones and dry plasma, achieving a δ^{87}Rb precision of ~0.03‰ (95% confidence interval) at Rb concentrations as low as 10 ppb. Our results also showed that Rb isotopic analysis is insensitive to sample/standard concentration mismatches within ±20% and variations in acid molarity from 0.15–0.75 mol L^{-1}. We also evaluated the impact of the MS/MS module on Rb isotopic analysis and found that enabling it reduced matrix effects from K. Our approach enables streamlined, simultaneous isotopic analysis of K and Rb isotopes from a single sample aliquot, offering new opportunities to explore the isotopic behaviors and fractionations of these elements across diverse geological, chemical, and biological processes.

Data availability

The data supporting this article have been included as part of the SI. See DOI: https://doi.org/10.1039/d5ja00189g.

Conflicts of interest

There are no conflicts to declare.

Acknowledgements

This work was supported by NASA grants (80NSSC23K1163 and 80NSSC24K1785), a Research Innovation Seed Fund and start-up funds provided by MIT to NXN. We thank Ryan Ickert and an anonymous reviewer for their constructive comments, which

greatly improved the manuscript, and Editor Tabitha Jay for her effective editorial handling.

References

1 S. M. McLennan, *Geochem., Geophys., Geosyst.*, 2001, **2**, 2000GC000109.
2 R. L. Rudnick and S. Gao, in *Treatise on Geochemistry*, ed. H. D. Holland and K. K. Turekian, Pergamon, Oxford, 2003, pp. 1–64, doi: DOI: 10.1016/B0-08-043751-6/03016-4.
3 D. Shaw, *Geochim. Cosmochim. Acta*, 1968, **32**, 573–601.
4 N. Dauphas, N. X. Nie, M. Blanchard, Z. J. Zhang, H. Zeng, J. Y. Hu, M. Meheut, C. Visscher, R. Canup and T. Hopp, *Planet. Sci. J.*, 2022, **3**, 29.
5 B. J. Wood, D. J. Smythe and T. Harrison, *Am. Mineral.*, 2019, **104**, 844–856.
6 Z. J. Zhang, N. X. Nie, R. A. Mendybaev, M.-C. Liu, J. J. Hu, T. Hopp, E. E. Alp, B. Lavina, E. S. Bullock, K. D. McKeegan and N. Dauphas, *ACS Earth Space Chem.*, 2021, **5**, 755–784.
7 N. X. Nie, X.-Y. Chen, T. Hopp, J. Y. Hu, Z. J. Zhang, F.-Z. Teng, A. Shahar and N. Dauphas, *Sci. Adv.*, 2021, **7**, eabl3929.
8 N. X. Nie, X.-Y. Chen, Z. J. Zhang, J. Y. Hu, W. Liu, F. L. H. Tissot, F.-Z. Teng, A. Shahar and N. Dauphas, *Geochim. Cosmochim. Acta*, 2023, **344**, 207–229.
9 N. X. Nie and N. Dauphas, *Astrophys. J., Lett.*, 2019, **884**, L48.
10 N. X. Nie, N. Dauphas, Z. J. Zhang, T. Hopp and M. Sarantos, *Sci. Adv.*, 2024, **10**, eadm7074.
11 V. Busigny, P. Cartigny, P. Philippot, M. Ader and M. Javoy, *Earth Planet. Sci. Lett.*, 2003, **215**, 27–42.
12 T. Zack and T. John, *Chem. Geol.*, 2007, **239**, 199–216.
13 M. Best, *Geology*, 1975, **3**, 429–432.
14 H. W. Nesbitt and G. Markovics, *Geochim. Cosmochim. Acta*, 1980, **44**, 1659–1666.
15 K. Wang, W. Li, S. Li, Z. Tian, P. Koefoed and X.-Y. Zheng, *Geochemistry*, 2021, **81**, 125786.
16 D.-S. Jiang, X.-T. Peng, W.-J. Xu, X. Hu, S. Erdmann, X.-S. Xu, G.-L. Zhang, C.-J. Pang, H.-C. Duan and F. Huang, *Earth Planet. Sci. Lett.*, 2024, **646**, 118978.
17 B. Wang, F. Moynier and Y. Hu, *Proc. Natl. Acad. Sci. U. S. A.*, 2024, **121**, e2311402121.
18 B. Wang, F. Moynier, M. G. Jackson, F. Huang, X. Hu, S. Ari Halldórsson, W. Dai and G. Devos, *Geochim. Cosmochim. Acta*, 2023, **354**, 38–50.
19 X. Zhang, L. Tang, J. Du, B. A. Haley, J. McManus, X. Hu and F. Huang, *Earth Planet. Sci. Lett.*, 2024, **642**, 118858.
20 K. Kossert and E. Günther, *Appl. Radiat. Isot.*, 2004, **60**, 459–464.
21 A. Grau Malonda and A. Grau Carles, *Appl. Radiat. Isot.*, 2002, **56**, 153–156.
22 N. X. Nie, D. Wang, Z. A. Torrano, R. W. Carlson, C. M. O. 'D. Alexander and A. Shahar, *Science*, 2023, **379**, 372–376.
23 Y. Zhang, S. Wang, J. Liu, B. Yang and L. Qin, *J. Anal. At. Spectrom.*, 2023, **38**, 1461–1468.
24 Y. Hu, X.-Y. Chen, Y.-K. Xu and F.-Z. Teng, *Chem. Geol.*, 2018, **493**, 100–108.
25 H. Chen, Z. Tian, B. Tuller-Ross, R. L. Korotev and K. Wang, *J. Anal. At. Spectrom.*, 2019, **34**, 160–171.
26 P. Télouk, E. Albalat, T. Tacail, F. Arnaud-Godet and V. Balter, *J. Anal. At. Spectrom.*, 2022, **37**, 1259–1264.
27 S. An, X. Luo and W. Li, *Rapid Commun. Mass Spectrom.*, 2022, **36**, e9289.
28 X. Li, G. Han, Q. Zhang and Z. Miao, *J. Anal. At. Spectrom.*, 2020, **35**, 1330–1339.
29 K. Hobin, M. Costas Rodríguez and F. Vanhaecke, *Anal. Chem.*, 2021, **93**, 8881–8888.
30 K. Hobin, M. Costas Rodríguez, E. Van Wonterghem, R. E. Vandenbroucke and F. Vanhaecke, *Anal. Chim. Acta*, 2024, **1315**, 342812.
31 L. E. Morgan, D. P. S. Ramos, B. Davidheiser-Kroll, J. Faithfull, N. S. Lloyd, R. M. Ellam and J. A. Higgins, *J. Anal. At. Spectrom.*, 2018, **33**, 175–186.
32 W. Li, B. L. Beard and S. Li, *J. Anal. At. Spectrom.*, 2016, **31**, 1023–1029.
33 H. Chen, N. J. Saunders, M. Jerram and A. N. Halliday, *Chem. Geol.*, 2021, **578**, 120281.
34 W. Li, M. Cui, Q. Pan, J. Wang, B. Gao, S. Liu, M. Yuan, B. Su, Y. Zhao and F.-Z. Teng, *Sci. China: Earth Sci.*, 2022, **65**, 1510–1521.
35 X.-Y. Zheng, X.-Y. Chen, W. Ding, Y. Zhang, S. Charin and Y. Gérard, *J. Anal. At. Spectrom.*, 2022, **37**, 1273–1287.
36 N. X. Nie, R. Grigoryan and F. L. Tissot, *J. Anal. At. Spectrom.*, 2024, **39**, 2038–2048.
37 E. Albalat, P. Télouk and V. Balter, *J. Anal. At. Spectrom.*, 2024, **39**, 2183–2191.
38 K. Wang and S. B. Jacobsen, *Geochim. Cosmochim. Acta*, 2016, **178**, 223–232.
39 F. M. Richter, R. A. Mendybaev, J. N. Christensen, D. Ebel and A. Gaffney, *Meteorit. Planet. Sci.*, 2011, **46**, 1152–1178.
40 F. M. Richter, E. B. Watson, M. Chaussidon, R. Mendybaev, J. N. Christensen and L. Qiu, *Geochim. Cosmochim. Acta*, 2014, **138**, 136–145.
41 F. Moynier, Y. Hu, K. Wang, Y. Zhao, Y. Gérard, Z. Deng, J. Moureau, W. Li, J. I. Simon and F.-Z. Teng, *Chem. Geol.*, 2021, **571**, 120144.
42 S. An, J. Chen, S. Boschi and W. Li, *Anal. Chem.*, 2023, **95**, 2140–2145.
43 Y. Hu, F. Moynier and M. Bizzarro, *Nat. Commun.*, 2022, **13**, 7669.
44 Y. Hu, F. Moynier and X. Yang, *Earth Planet. Sci. Lett.*, 2023, **620**, 118319.
45 N. X. Nie, N. Dauphas, T. Hopp, J. Y. Hu, Z. J. Zhang, R. Yokochi, T. J. Ireland and F. L. Tissot, *J. Anal. At. Spectrom.*, 2021, **36**, 2588–2602.
46 Y. Q. Zhang, W. Wei, Z. Zhang, X. Hu, H. M. Yu and F. Huang, *Geostand. Geoanal. Res.*, 2025, **49**, 259–270.
47 E. A. Pringle and F. Moynier, *Earth Planet. Sci. Lett.*, 2017, **473**, 62–70.
48 O. Nebel, K. Mezger, E. Scherer and C. Münker, *Int. J. Mass Spectrom.*, 2005, **246**, 10–18.
49 X. Hu, X.-Y. Nan, H.-M. Yu and F. Huang, *J. Anal. At. Spectrom.*, 2021, **36**, 2744–2755.

50 Z. Zhang, J. Ma, L. Zhang, Y. Liu and G. Wei, *J. Anal. At. Spectrom.*, 2018, **33**, 322–328.
51 N. Dauphas, J. H. Chen, J. Zhang, D. A. Papanastassiou, A. M. Davis and C. Travaglio, *Earth Planet. Sci. Lett.*, 2014, **407**, 96–108.
52 N. Dauphas, T. Hopp, G. Craig, Z. J. Zhang, M. C. Valdes, P. R. Heck, B. L. A. Charlier, E. A. Bell, T. M. Harrison, A. M. Davis, L. Dussubieux, P. R. Williams, M. J. Krawczynski, C. Bouman, N. S. Lloyd, D. Tollstrup and J. B. Schwieters, *J. Anal. At. Spectrom.*, 2022, **37**, 2420–2441.
53 A. Gale, C. A. Dalton, C. H. Langmuir, Y. Su and J.-G. Schilling, *Geochem., Geophys., Geosyst.*, 2013, **14**, 489–518.
54 W. Li, Y. Zhao, B. Su, B. Gao, J. Wang and S. Liu, *J. Anal. At. Spectrom.*, 2023, **38**, 603–608.